HHS Public Access

Author manuscript

J Comp Neurol. Author manuscript; available in PMC 2017 November 15.

Published in final edited form as:

J Comp Neurol. 2017 June 15; 525(9): 2235–2248. doi:10.1002/cne.24202.

A comparative analysis of the physiological properties of neurons in the anterolateral bed nucleus of the stria terminalis in the *Mus musculus*, *Rattus norvegicus*, and *Macaca mulatta*

Sarah E. Daniel[1,2], **Jidong Guo**[1,2], and **Donald G. Rainnie**[1,2]

[1]Behavioral Neuroscience and Psychiatric Disorders, Yerkes National Primate Research Center, Atlanta, Georgia

[2]Department of Psychiatry and Behavioral Science, Emory University School of Medicine, Atlanta, Georgia

Abstract

The anterolateral group of the bed nucleus of the stria terminalis ($BNST_{ALG}$) is a critical modulator of a variety of rodent and primate behaviors spanning anxiety behavior and drug addiction. Three distinct neuronal cell types have been previously defined in the rat $BNST_{ALG}$ based on differences in the voltage-response to hyperpolarizing and depolarizing current injection. Differences in genetic expression profile between these three cell types suggest electrophysiological cell type may be an indicator for functional differences in the circuit of the rat $BNST_{ALG}$. Although the behavioral role of the BNST is conserved across species, it is unknown if the same electrophysiological cell types exist in the $BNST_{ALG}$ of the mouse and nonhuman primate. Here, we used whole-cell patch clamp electrophysiology and neuronal reconstructions of biocytin-filled neurons to compare and contrast the electrophysiological and morphological properties of neurons in the $BNST_{ALG}$ from the mouse, rat, and rhesus macaque. We provide evidence that the $BNST_{ALG}$ of all three species contains neurons that match the three defined cell types found in the rat; however, there are intriguing differences in the relative frequency of these cell types as well as electrophysiological and morphological properties of the $BNST_{ALG}$ neurons across species. This study suggests that the overall landscape of the $BNST_{ALG}$ in the primate and mouse may be similar to that of the rat in some aspects but perhaps significantly different in others.

Graphical Abstract

Correspondence: Donald G. Rainnie, Psychiatry and Behavioral Neuroscience, Emory University School of Medicine, 954 Gatewood Rd NE, Yerkes Neuroscience Building, Atlanta, GA 30327. drainni@emory.edu.

CONFLICT OF INTEREST STATEMENT

The authors have no conflict of interest to report.

ROLE OF THE AUTHORS

All authors had full access to all of the data in the study and take responsibility for the integrity of the data and the accuracy of the data analysis. Study concept and design: SED. Acquisition of data: SED and JDG. Analysis and interpretation of data: SED, JDG, and DGR. Drafting of the manuscript: SED. Critical revision of the manuscript for important intellectual content: DGR. Statistical analysis: SED. Obtained funding: DGR. Study supervision: DGR.

Using in vitro patch clamp recording from neurons in the anterolateral bed nucleus of the stria terminalis ($BNST_{ALG}$) of the mouse, rat, and rhesus macaque, the authors show species differences in both the proportion of cell types recorded and their electrophysiological properties.

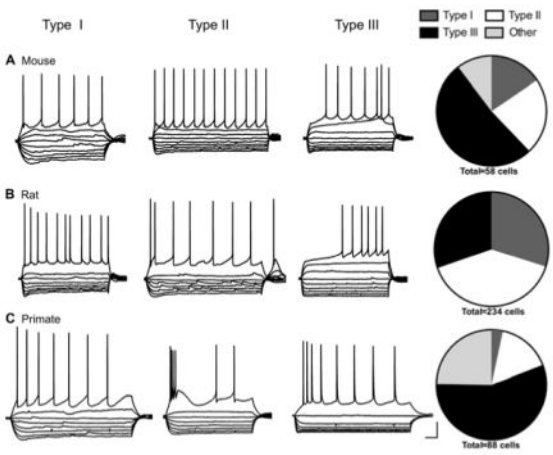

Keywords

extended amygdala; morphology; mouse; nonhuman primate; patch-clamp electrophysiology; rat; RRID: AB_2315383; RRID: SCR_001622; RRID: SCR_001775; RRID: SCR_002798

1 | INTRODUCTION

There is a growing literature that describes the importance of the anterior bed nucleus of the stria terminalis (BNST) in a variety of behaviors including anxiety behavior and drug addiction (Duvarci, Bauer, & Pare, 2009; Kalin, Shelton, Fox, Oakes, & Davidson, 2005; Mantsch et al., 2014; Pleil, Rinker, et al., 2015; Sullivan et al., 2004). Although most of this research has been done in rodents, there is also evidence from both human and nonhuman primate studies that supports the role of the BNST as a modulator of anxiety behavior, drug self-administration, binge alcohol drinking, threat monitoring, and anticipatory anxiety (Alvarez, Chen, Bodurka, Kaplan, & Grillon, 2011; Fox et al., 2010; Macey, Smith, Nader, & Porrino, 2003; Pleil, Lowery-Gionta, et al., 2015; Somerville, Whalen, & Kelley, 2010; Straube, Mentzel, & Miltner, 2007). These studies strongly indicate that the role of the BNST is conserved across species from the rodent to the primate, suggesting the structure of the BNST may be conserved as well.

The BNST is not a homogenous structure; the rat BNST can be divided into at least 16 unique subregions and contains numerous distinct cell populations (Bota, Sporns, & Swanson, 2012; Dong, Petrovich, Petrovich, Watts, et al., 2001; Dong & Swanson, 2004; Ju, Swanson, & Simerly, 1989; Larriva-Sahd, 2006). The heterogeneity of the neurons in the BNST has been studied in depth in the anterolateral group of the BNST ($BNST_{ALG}$) of the rat. Most neurons in $BNST_{ALG}$ of the rat can be classified into three distinct cell types based on their spiking and rectification properties and rebound depolarization in response to hyperpolarizing and depolarizing current injection: Type I (regular spiking [RS]), Type II

(low-threshold bursting [LTB]), and Type III (fast inward rectifiers; Hammack, Mania, & Rainnie, 2007; Rodriguez-Sierra, Rodríguez-Sierra, Turesson, & Pare, 2013). Importantly, these cell types differ in their expression profile of messenger RNA (mRNA) for ion channel subunits, serotonin receptor subtypes, and the neuropeptide, corticotropin releasing factor (CRF) (Dabrowska, Hazra, Guo, Li, et al., 2013; Guo, Hammack, Hazra, Levita, & Rainnie, 2009; Hazra et al., 2011). Hence, the electrophysiological cell type of neurons in the $BNST_{ALG}$ may be indicative of the functional role the neurons play in the circuit. Indeed, the vast majority of Type III neurons in the rat $BNST_{ALG}$ express the mRNA for CRF and are affected by stress in different ways than Type I and Type II cells (Dabrowska, Hazra, Guo, Li, et al., 2013), providing further evidence that cell types play different roles in the circuit.

Although Type I, Type II, and Type III cells were defined in the $BNST_{ALG}$ of the rat, the classification system has been appropriated for describing neurons in the mouse BNST (Silberman, Matthews, & Winder, 2013). Because the role of the BNST in anxiety behavior is conserved across multiple species, it is assumed that the neurons in the mouse BNST are similar to that of the rat. However, no study has systematically examined the neurons of the mouse $BNST_{ALG}$ to determine if the classification system defined in the rat is appropriate for describing neuron-heterogeneity in the mouse. Similarly, it is unknown if the electrophysiological cell types of the rat $BNST_{ALG}$ are conserved in the BNST of the primate.

Here, we used whole-cell patch clamp electrophysiology to describe the electrophysiological properties of $BNST_{ALG}$ neurons in the mouse, rat, and rhesus macaque using the classification system initially described in the rat (Hammack et al., 2007). We, then, compared and contrasted the physiological properties of neurons of the same cell type in the three species. Furthermore, we described the characteristics of neurons that do not fit the classic description of a Type I, Type II, or Type III cell. Finally, we filled neurons with biocytin for post hoc morphological reconstruction and analysis to compare the dendritic arbor of $BNST_{ALG}$ neurons in the three species.

2 | METHODS

2.1 | Animal subjects

All procedures were approved by the Institutional Animal Care and Use Committee of Emory University and were in compliance with National Institute of Health guidelines. For rats, recordings were performed in male Sprague-Dawley rats aged 40–60 days old (n =63; Charles River Laboratories, Wilmington, MA). For mice, recordings were performed in wild-type C57BL/6 male mice (n =13). Three to five neurons were recorded per animal. Animals were housed in same-sex groups, two to four rats per cage, and two to six mice per cage. Rats and mice were maintained on a 12 : 12-hr light-dark cycle with ad libitum access to food and water.

The primate tissue for this study was obtained from male juvenile (14–40 months) *Macaca mulatta* monkeys (n =9). Due to the limited availability of primate tissue, we recorded more neurons per animal than that recorded in the rat or mouse, ranging from 8 to 12 per primate.

The primates were born into the breeding colony housed at the Yerkes National Primate Research Center Field Station and raised in normal social groups. They were provided with ad libitum access to food and water and monitored by the Yerkes veterinary staff. Animals used in this study were selected for sacrifice by the veterinary staff for failure to thrive and/or chronic diarrhea refractory to treatment as part of the animal care end-points approved for our monkey colony. Once identified, the animals were moved to the Yerkes Main Station and scheduled for sacrifice within the week.

2.2 | Preparation of BNST slices

2.2.1 | Preparation of mouse and rat BNST slices—BNST slices were obtained as previously described for rats (Hammack et al., 2007). The same procedure was done for mice. Briefly, rodents were decapitated under isoflurane anesthesia (Med-Vet International, Mettawa, IL), and the brains were rapidly removed and placed in ice-cold kynurenic acid-based "cutting solution" which contained (mM): NaCl (130), KCL (3.50), KH_2PO_4 (1.10), $MgCl_2$ (6.0), $CaCl_2$ (1.0), glucose (10), supplemented with kynurenic acid (2.0). Coronal sections containing BNST were cut 350-μm thick using a Leica VTS-100 vibratome (Leica Microsystems, Bannockburn, IL). Slices were kept in oxygenated cutting solution at room temperature for 1 hr before transferring to regular artificial cerebrospinal fluid (ACSF) containing (mM): NaCl (130), $NaHCO_3$ (30), KCl (3.50), KH_2PO_4 (1.10), $MgCl_2$ (1.30), $CaCl_2$ (2.50), and glucose (10). Slices were kept in oxygenated ACSF for at least 30 min before recording.

2.2.2 | Preparation of rhesus macaque BNST slices—The primate BNST slices were obtained as previously described (Muly et al., 2009; Ryan et al., 2012). The animals were sacrificed with an overdose of pentobarbital (100 mg/kg) and hand-cut blocks of tissue were mounted on a vibratome and 350 μm coronal slices were cut as previously described (Muly et al., 2009). Slices were then treated the same as the mouse and rat BNST slices: first kept in oxygenated cutting solution for 1 hr before transferring to ACSF.

2.3 | General patch clamp recording procedures

Individual slices were transferred to a recording chamber mounted on the fixed stage of a Leica DM6000 FS microscope (Leica Microsystems Inc., Bannockburn, IL) equipped with an IR sensitive CCD camera (Orca ER, Hamamatsu, Tokyo, Japan), allowing for use of differential interference contrast (DIC) optics and infrared illumination to identify individual BNST neurons. The slices were maintained fully submerged and continuously perfused with oxygenated 32°C ACSF with a speed of ~2 ml/min. All recordings were confined to the dorsal anterolateral cell group including the oval, juxtacapsular, and anterolateral nucleus of the BNST ($BNST_{ALG}$; Figure 1). This region has a triangular shape and is landmarked by three distinct structures including the internal capsule, the lateral ventricle, and the anterior commissure. Furthermore, all neurons recorded were lateral to the stria terminalis to avoid medial BNST neurons. The delineation of the anterolateral and anteromedial regions of the BNST in the rhesus macaque is not well defined, so recordings were limited to the trianglular region corresponding to the anterolateral BNST as best as possible. Whole-cell recordings were obtained using recording pipettes pulled from borosilicate glass and having a resistance of 4–6 MΩ. Pipettes were filled with a potassium-based patch solution

containing the following (mM): K-gluconate (130), KCl (2), HEPES (10), $MgCl_2$ (3), K-ATP (2), Na-GTP (0.2), and phosphocreatine (5), and was titred to pH 7.3 with KOH and 290 mOsm. Biocytin (0.3%) was added to the patch solution in some cases to allow for post hoc histochemical processing and neuronal reconstruction.

2.3.1 | Analysis of electrophysiological properties—Basic electrophysiological properties were collected from each cell recorded. A DC holding current was injected to maintain the membrane potential at −60 mV in current clamp. To characterize neurons, a series of 10 hyperpolarizing and depolarizing, 750 or 1000 ms long, square-wave current steps was injected and scaled so that the peak negative voltage deflection was to approximately −80 mV (Hammack et al., 2007; Hazra et al., 2011). Then, linear ramps of depolarizing current were injected, lasting 250 ms, and scaled to depolarize the neuron to elicit a single action potential. Data were analyzed by importing the raw voltage and current traces into Matlab (The MathWorks, Narick, MA; RRID: SCR_001622) using scripts provided with sigTOOL (http://sigtool.sourceforge.net/, developed at King's College London) and processed with customized scripts (available upon request).

Analysis of electrophysiological properties was completed as described elsewhere (Ehrlich, Ryan, & Rainnie, 2012). Briefly, input resistance (R_{in}) was calculated using the deflection in response to the smallest hyperpolarizing current step (~5 mV) and calculated as the ratio of peak voltage deflection to the current injected. The I_h score was calculated as the ratio of the magnitude of I_h (measured as peak deflection at the beginning of the trace minus steady state at the end) to the membrane potential at the point of peak deflection in the trace with the peak deflection closest to −80 mV (smaller positive values indicate less voltage deflection due to I_h). The $I_{K(IR)}$ score was calculated as the ratio of the peak magnitude of the smallest hyperpolarizing trace to the difference between the peak-magnitude of the two most hyperpolarizing traces (larger values indicate more inward rectification). Because all of these measurements require a relatively stable membrane potential at a particular portion of the voltage trace, cells with unstable membrane potentials at the necessary time points were removed for these analyses. The latency to the first action potential was calculated as the duration of time after the initiation of the depolarizing current step and before the first action potential. If the latency to the first action potential was >750 ms, it was not used in the analysis as most cells only had current steps 750 ms long.

2.4 | Neuronal morphology

2.4.1 | Histochemical processing—Some of the patched neurons were labeled with 0.3% biocytin (Sigma Aldrich, St Lois, MO) included in the patch pipette recording solution and used for neuronal reconstruction as previously described (Ryan, Ehrlich, & Rainnie, 2014). One to two neurons per mouse and rat and three to four neurons per primate were labeled. After neurons were recorded for at least 10 min, slices were fixed in 10% buffered formalin (Fisher Scientific, Hanoverpark, IL) for 12–72 hr, and then transferred to cryoprotectant for storage at −20°C. After three consecutive 10 min washes in 0.05 M phosphate buffered saline (PBS), slices were permeabilized for 30 min in PBS containing 0.5% Triton-X 100 (Sigma-Aldrich, St Louis, MO). Slices were then treated with Alexa Fluor 488- or 568-conjugated Streptavidin (Invitrogen, Grand Island, New York; RRID:

AB_2315383) diluted to 1 : 1,000 in PBS with Triton-X for 36–48 hr at 4°C. Slices were then washed two times for 1 hr each in 0.05 M PBS and washed for 10 min in 0.05 M phosphate buffer. The slices were then mounted on glass slides, air dried for 3–12 hr, and cover-slipped with mowiol mounting medium (Sigma-Aldrich, St Louis, MO).

2.4.2 | Neuronal reconstruction and analysis—Z-stack images of the biocytin-filled neurons were taken at either 10× or 20× magnification with a 0.4 or 0.3 μm step size, respectively, using a Leica DM5500B spinning disk confocal microscope (Leica Microsystems Inc., Bannockburn, IL) and SimplePCI data acquisition software (Compix, Sewickley, PA). For morphological analysis, the dendritic arbor and cell body of each neuron was reconstructed by hand using Neurolucida neuron tracing software (MicroBrightField, Colchester, VT; RRID: SCR_001775). Quantitative analysis of reconstructions, including total dendritic length, number of dendritic ends, and cross-sectional area of soma, was performed using Neurolucida Explorer (MicroBrightField).

2.5 | STATISTICAL ANALYSIS

Statistical analyses were carried out using Prism 6 (GraphPad Software Inc., San Diego, CA; RRID: SCR_002798). The relative frequency of cell types was compared using a χ^2-test when samples being compared had >10 cells per cell type. Due to the small sample size of some data sets, normality was estimated by visual discrimination. For data sets with a normal distribution, an ordinary one-way ANOVA (when not dividing by cell type) or two-way ANOVA (with cell type and species as the two factors) with Tukey's multiple comparisons test was used. For data sets with a non-normal distribution, such as input resistance, a Kruskal-Wallis test with Dunn's multiple comparisons test was used. An alpha level of 0.05 was used for all statistical tests, and data are presented as mean ± *SEM*.

3 | RESULTS

3.1 | Comparative physiology of type I–III neurons

For this study, we recorded electrophysiological properties from neurons in the $BNST_{ALG}$ (Figure 1) of the mouse (n = 56 cells from 13 mice), rat (n =234 cells from 63 rats), and rhesus macaque (n =89 cells from nine primates). Neurons that fit the classification system previously defined in the rat were divided into three groups based on a visual discrimination of current clamp traces showing the voltage response to hyperpolarizing and depolarizing square-wave current injections, as previously described (Hammack et al., 2007). Type I neurons were characterized by a depolarizing sag in response to hyperpolarizing current injection indicative of an I_h current and a steady firing rate, but did not exhibit low-threshold depolarizing waves or burst-firing activity. In contrast, Type II neurons exhibited rebound spiking after the hyperpolarizing current steps, burst firing activity, and/or a prevalent low-threshold depolarizing wave indicative of a prominent I_T current. Finally, Type III cells were classified based on the presence of a pronounced fast inward rectification in response to hyperpolarizing current injection indicative of an inwardly rectifying potassium current ($I_{K(IR)}$) and did not exhibit any signs of an I_T current and little-to-no I_h current (Figure 2). Neurons that did not fit into these cell types were classified as "others" and will be described in more detail below.

3.1.1 | Type I cells—Type I neurons were originally defined in the rat as cells that exhibit an I_h current resulting in a depolarizing sag in response to hyperpolarizing current injections and do not exhibit burst firing activity (Hammack et al., 2007). Although cells that meet this description were found in both the mouse and primate $BNST_{ALG}$, the proportion of cells classified as Type I was significantly reduced from that seen in the rat (Figure 2). There was a significant overall effect of cell type for both the I_h and $I_{K(IR)}$ scores: Type I cells had significantly larger I_h scores than Type III cells but smaller than Type II cells in all species (Type I: 0.046 ±0.002, Type II: 0.057 ±0.002, Type III: 0.014 ±0.001; $p < .0001$, $F_{(2, 339)} = 49.67$; Figure 3a), and Type I and Type II cells had a significantly lower $I_{K(IR)}$ score than Type III cells (Type I: 2.11 ± 0.12, Type II: 2.12 ± 0.10, Type III: 3.76 ±0.19; $p < .0001$, $F_{(2, 338)} = 13.52$; Figure 3b). However, the properties of Type I cells did not differ much between species (Table 1). Although there was a significant effect of species for action potential threshold and latency to first spike (threshold: $p < .001$, $F_{(2, 334)} = 9.33$; latency to first spike: $p < .05$, $F_{(2, 339)} = 3.61$), multiple comparisons test did not show a difference between species in the Type I cells (Figure 3c,d). Additionally, there was no difference in the input resistance (R_{in}) of Type I cells between mouse and rat (Table 1). The low sample size ($n = 3$; from three different primates) of primate Type I cells and wide variance in the R_{in} made it impossible to compare across species. There was no overall effect of species on the I_h score ($p = .070$, $F_{(2, 339)} = 2.586$; Figure 3a); however, the I_h scores in the mouse Type I cells were generally smaller than that seen in the rat Type I cells ($p < .05$).

3.1.2 | Type II cells—Type II cells are distinguished by the presence of a voltage-dependent calcium current (I_T) that causes re-bound firing after hyperpolarizing current injections and/or a low-threshold calcium wave at the beginning of depolarizing current injections. Type II cells are the most common cell type in the rat but only represented about 22 and 16% of the cells in the mouse and primate $BNST_{ALG}$, respectively (Figure 2 and Table 2). This included cells that had any indication of a prominent I_T, including cells that did not show any noticeable I_h. Indeed, less than half of the primate Type II cells exhibited signs of an I_h current. Unsurprisingly then, the I_h score was significantly smaller in primate Type II cells than the I_h score in Type II rat cells (primate Type II: 0.046 ± 0.010, rat Type II: 0.059 ±0.002; $p < .05$, Figure 3a). Unlike the primate Type II cells, 12 of the 13 Type II cells in the mouse $BNST_{ALG}$ had a depolarizing sag in response to hyperpolarizing current. However, the I_h score in the mouse Type II cells was also significantly smaller than that in the rat (mouse Type II: 0.033 ±0.006, $p < .05$).

In addition to the variable size of the I_h current, the I_T current also varied between species. Often the I_T in the mouse Type II cells was only seen as a small depolarizing current at the beginning of the depolarizing step without initiating action potentials (Figure 2a). In contrast, primate Type II cells often had many spikes on top of the low-threshold calcium wave (Figure 2c). Rebound firing after a hyperpolarizing current injection was most common in rat Type II cells with 8 out of 33 (about 24%) exhibiting rebound firing, followed by primate Type II cells with 2 out of 14 cells (about 14%) and mouse Type II cells with 1 out of 13 cells (about 8%). This suggests the I_T current was potentially weaker in mouse Type II cells than the I_T in rat and primate Type II cells.

There was no significant difference in the R_{in}, threshold for action potential generation, latency to first spike, or $I_{K(IR)}$ score between Type IIs of different species (Figure 3a,c,d, Table 1). However, there was a significant difference in how the threshold for action potential generation in Type II cells related to other cell types within the same species. In addition to the significant effect of species on threshold, there was a significant effect of cell type ($p < .001$, $F_{(2, 334)} = 7.33$) and an interaction of the two ($p < .01$, $F_{(4, 334)} = 3.738$). In both the mouse and rat, Type II cells had a lower threshold for action potential generation than Type III cells ($p < .001$ and $p < .0001$, respectively, Table 1) and in this sample of rat neurons, Type II cells also had a lower threshold for action potential than the Type I cells ($p < .001$). In contrast, there was no significant difference in threshold for action potential between Type I, Type II, and Type III cells in the primate (Figure 3c).

3.1.3 | Type III cells—The physiological profile of Type III cells seems to be the most conserved across the three species. Type III cells were seen in all three species and were the most common cell type in both the mouse and primate (Figure 2). In all species, there was a significant population of cells in the BNST that displayed a strong fast inward rectification in response to hyperpolarizing current injection without low-threshold spiking or burst firing activity. This was reflected in the significantly higher $I_{K(IR)}$ score seen in Type III cells compared to Type I and Type II cells as reported above (Figure 3b). Additionally, these neurons tended to only exhibit a small, fast depolarizing sag indicative of either little-to-no I_h current or an I_h current with faster kinetics than that found in Type I and Type II neurons. This is reflected in the smaller I_h score seen in all Type III cells compared to both Type I and Type II cells regardless of species (statistics reported above; Figure 3a).

Although the electrophysiological phenotype of Type III neurons from the three species looked very similar, there were some notable differences. First, there was a significant effect of cell type ($p < .0001$, $F_{(2, 339)} = 13.26$), species ($p < .05$, $F_{(2, 339)} = 3.61$), and an interaction of the two ($p < .05$, $F_{(4, 339)} = 2.58$) on the latency to the first spike with a depolarizing current injection. Specifically, the latency shortened from mouse (314 ±32.3 ms) to rat (224.5 ±19.7 ms) to primate in Type III cells (154.3 ±14.1 ms; mouse vs. rat $p < .01$; mouse vs. primate $p < .0001$; rat vs. primate $p < .01$, Figure 3d). A long latency to the first spike is indicative of a voltage-dependent potassium current such as I_A or I_D (Francesconi et al., 2009; Molineux, Fernandez, Mehaffey, & Turner, 2005). It is possible that the amount of I_A or I_D current varies significantly between species. However, the threshold for action potential generation also varied significantly across the three species, decreasing from mouse (−31.9 ±0.7 mV) to rat (−34.6 ±0.5) to primate (−38.5 ±0.7 mV; mouse vs. rat $p < .01$, mouse vs. primate $p < .0001$, rat vs. primate $p < .0001$; Figure 3c). The shorter latency to the first action potential in primate Type III cells may be due to a lower threshold for action potential generation. Finally, there was also a difference in the R_{in} of type III cells ($p < .0001$, Kruskal-Wallis statistic =49.52), and both the mouse (277.1 ±27.0 MΩ) and rat Type III cells (336.1 ±28.1 MΩ) had a significantly higher input resistance than the Type III cells from the primate (141.1 ±15.0 MΩ, $p < .0001$ for both comparisons; Table 1).

3.2 | Comparative frequency of cell types in the $BNST_{ALG}$

3.2.1 | Comparison of the current rat sample with previous published rat samples—

Here, we used a sample of 234 neurons (from 63 rats) in the rat $BNST_{ALG}$ as a basis from which to compare the properties of neurons recorded from the mouse and primate BNST. However, we first wanted to determine if the relative frequency of the cell types observed in this large sample differed from what has been reported in previous samples from our lab (Hammack et al., 2007; Hazra et al., 2011). As illustrated in Table 2, the current sample had a significantly different relative frequency of cell types from that seen in our original study describing the three cell types (χ^2 =39.46, p <.0001; Hammack et al., 2007). However, the relative frequency of the observed cell types differed between other samples collected within our lab as well (Table 2; Hazra et al., 2011). Importantly, there is a common trend observed across all sample populations; Type II cells are the most common cell type, ranging from 40 to 66% of $BNST_{ALG}$ neurons. The relative percentage of Type I and Type III cells varies between studies with Type I cells reported as 11–30% of the population, and Type III cells as 16–30% of the population.

3.2.2 | Relative frequency of cell types in the mouse—

Here, we examined the relative frequency of Type I, Type II, and Type III neurons in a sample of 56 cells from 13 mice. Notably, the relative frequency of cell types in the mouse was different from that observed in the rat (Figure 2a,b). Unlike the rat where Type II cells were the most prominent phenotype, Type III cells were the most common cell type in the mouse $BNST_{ALG}$ with 54% of neurons exhibiting strong fast-inward rectification (Figure 2a).

Additionally, 6 out of the 56 cells recorded did not adequately meet the criteria for Type I, Type II, or Type III neurons, and were therefore labeled as “other” (Figure 4a). Of those six, four cells (about 7% of total population) were RS neurons similar to Type I and Type III cells; however, unlike Type I cells, they did not exhibit a depolarizing-sag, and unlike Type III cells, they did not exhibit fast-inward rectification with hyperpolarizing current injection (Figure 4b). The final two mouse cells were different from each other but did not conform to any of the previously defined cell types. Both cells had strong fast-inward rectification and a small, slow depolarizing sag with hyperpolarizing current injections (Figure 4c,d). Although the fast-inward rectification would point toward these neurons being Type III cells, Type III cells of the rat and those identified here as mouse Type III cells have either no depolarizing-sag or a small but fast depolarizing sag. Additionally, the spiking pattern was different than the typical Type III cell. The first cell (Figure 4c) showed a RS pattern with a small amount of spike frequency adaptation, however, the action potential waveform was unique with a large fast after hyperpolarization (fAHP). This unique spike characteristic and slow depolarizing-sag made this cell stand apart from Type III neurons while the fast-inward rectification prevented it from being classified as a Type I neuron. The second cell (Figure 4d) exhibited spike accommodation. In the rat, 5 out of 70 Type I cells and 1 out of 71 Type III cells showed spike accommodation; however, in these cases the fast-inward rectification and depolarizing-sag corresponded more closely to that of a particular cell type. For this reason, this cell is not included in the cell classification.

3.2.3 | Relative frequency of cell types in the rhesus macaque—Here, we examined the relative frequency of Type I, Type II, and Type III neurons in a sample of 89 neurons from nine rhesus macaques. While neurons with similar electrophysiological phenotypes as rat Type I, Type II, and Type III cells were observed in the anterolateral region of the BNST of the rhesus macaque, only 75% of the cells recorded could be classified in those terms (Figure 2c). Intriguingly, like the mouse BNST, the majority of primate neurons (56%) recorded fit the description for Type III cells.

Only 3 out of 89 cells in the primate BNST had the characteristics of Type I cells including a regular firing rate, depolarizing-sag in response to hyperpolarizing current, and little-to-no fast inward rectification. There were nine other cells (about 10% of the total population) that showed a regular firing rate similar to that of Type I cells, however these cells did not exhibit the depolarizing-sag indicative of an I_h current or strong fast-inward rectification (Figure 5b). For this reason, these cells were categorized as “other.”

Whereas Type II cells are the most common cell type in the rat, only about 16% of the cells in the primate could be classified as Type II. Type II cells are characterized by the presence of an observable I_T current, either in the form of rebound firing after the hyperpolarizing step, or calcium waves visible at the beginning of the depolarizing step, with or without additional spikes. Type II cells of the rat also have a depolarizing-sag with hyperpolarizing current injections, indicative of an I_h current. Here, only six cells (6.8% of total) had an observable I_h current and depolarizing-sag. However, because the defining characteristic of a Type II cell is the presence of an I_T current, we included cells that showed an I_T current but little-to-no depolarizing-sag. Using these criteria, 14 (15.9%) of the primate neurons were classified as Type II.

The remaining 25% of cells from the primate that did not fit into the Type I–III classification were grouped into four categories: RS without indications of I_h or $I_{K(IR)}$ (as described above, about 10% of total population), cells with a large fast afterhyperpolarizing potential (fAHP) and medium afterhyperpolarizing potential (mAHP) (about 9% of total population), cells with a stuttering firing pattern (about 4.5% of total population), and cells with low-threshold calcium spikes (about 2% of the population; Figure 5). Unlike the cell with the large fAHP seen in the mouse, the cells with the large fAHP in the primate had a relatively slow firing rate, with an average of 5.8 spikes/s compared to 20 spikes/s in the mouse cell with the large fAHP (Figure 5c). Besides the slow firing rate and large fAHP, these cells differed from one another in other characteristics; for example, four out of the eight large fAHP primate cells exhibited the depolarizing sag indicative of an I_h current, and one cell exhibited fast inward rectification in response to the hyperpolarizing current. However, the consistent action potential waveform set these cells apart from the other cell types. Another group of primate cells that did not fit into our classification criteria exhibited repeated low-threshold calcium spikes in response to one depolarizing current pulse (Figure 5d). One of the two cells that exhibited this phenotype also had spontaneous low-threshold calcium spikes when held at −60 mV (not shown). The relative low frequency of this cell type calls into question its prevalence in the primate $BNST_{ALG}$; more recordings would need to be done to confirm if there is indeed a consistent presence of these cells.

The final group of primate cells seen displayed a unique stutter-firing pattern (Figure 5e). These cells looked similar to Type III cells in that they had little-to-no depolarizing sag in the hyperpolarizing traces and had strong inward rectification, however, they did not exhibit a regular firing pattern. At the more depolarizing current steps, these cells fired two to seven action potentials at a rate ranging from 37 to 75 spikes/s followed by an abrupt break in firing before another period of rapid spikes. These spikes did not occur on calcium waves but rather were initiated from a steady membrane potential. Additionally, each spike was followed by a large fAHP and mAHP, giving them a unique spike waveform. Of the outlying cell types, this was the most unique phenotype that has never been reported in the mouse or rat BNST.

3.3 | Morphology and input resistance

In previous studies, our lab has not seen any correlation between morphology of rat $BNST_{ALG}$ neurons and their electrophysiological phenotype, and another independent study confirmed this observation (Rodriguez-Sierra et al., 2013). For this reason, we present data on the neuronal morphology with all cell types combined. Here, 12 mouse (n =9 mice), 11 rat (n =6 rats), and 14 primate (n =5 primates) biocytin-filled neurons were traced using Neurolucida (MicroBright-Field, Colchester, VT) to provide us with a measure for total dendritic length, number of dendrites, number of dendritic branches, and cross-sectional area of the soma. A schematic diagram summarizing the relative location of the recording sites of each of the neurons is illustrated in Figure 1a. As seen in Figure 6a–c, the dendritic arbor of the representative primate neuron was more complex than that of the neurons from the mouse and rat $BNST_{ALG}$. There was a significant difference among the dendritic length in all species (p <.0001, $F_{(2, 33)}$ = 24.86) with primate neurons having significantly longer total dendritic length (2842 ±241.3 μm) than the neurons from the rat (1810 ±159.5 μm; p <.01) and mouse (935.9 ±122.4 μm; p <.0001) and the rat having significantly longer total dendritic length than the neurons from the mouse (p <.05; Figure 6d). Although there was no difference in the number of dendrites between species (p =.13, $F_{(2, 33)}$ = 2.195), there was a significant difference in the number of dendritic ends (p <.001, $F_{(2, 33)}$ = 10.57) with primate neurons having significantly more (19.4 ± 1.9 ends) than both mouse (9.64 ±1.3 ends, p <.001) and rat (11.8 ± 1.2 ends, p <.01), indicating there was more dendritic branching in the primate $BNST_{ALG}$ neurons (Figure 6e). On the other hand, there was no difference in the cross-sectional area of the soma between cell types (p =.16, $F_{(2, 33)}$ = 1.915; Figure 6f).

Because a change in morphology is tightly associated with a change in R_{in}, we looked to see if the membrane input resistance in primate cells decreased as would be predicted by the increase in the size of the dendritic arbor (Barrett & Crill, 1974). Interestingly, there was a significant difference in R_{in} between species (p < .01, Kruskal-Wallis statistic =15.82); however, a multiple comparisons test showed that only the R_{in} from the rat $BNST_{ALG}$ neurons was significantly higher than the R_{in} from the primate cells (rat: 349.8 ± 12.9 MΩ, primate: 340.4 ±37.8 MΩ; p <.01). However, R_{in} is highly variable, especially between multiple cell types. As described above, the primate Type III cells had significantly lower R_{in} than the Type III cells of both the mouse and rat (Figure 6g).

4 | DISCUSSION

Here, we showed that neurons matching the electrophysiological phenotype of the cell types defined in the rat $BNST_{ALG}$ were also found in the $BNST_{ALG}$ of the mouse and rhesus macaque; however, these cell types were found in different proportions than had been reported previously in the rat $BNST_{ALG}$ and did not adequately describe the entire population. In the rat, Type II cells were the most common cell type ranging from 38–66% of all $BNST_{ALG}$ neurons. In contrast, they only represented 22% of mouse neurons and 16% of primate $BNST_{ALG}$ neurons. In both the mouse and primate, Type III cells, with strong fast inward rectification, were the most common cell type observed, describing 51% of cells in the mouse and 56% in the primate compared to only 27% of cells in the rat $BNST_{ALG}$. Moreover, although there were similarities in the physiological properties of BNST neurons across species, this study suggested that the overall landscape of the $BNST_{ALG}$ in the primate and even mouse may differ from that of the rat.

Significantly, the classification of cell types in the rat BNST has been independently verified by Pare and colleagues (Table 2, Rodriguez-Sierra et al., 2013). Here, the authors looked at the distribution of cell types in the anterior BNST across the anterolateral, anteromedial, and anteroventral regions. They reported LTB (matching our description of Type II cells) and RS (matching the description of Type I cells) were the two most common cell types found in all three regions of the anterior BNST. A cell type matching our classification of Type III cells was defined as fast-inward rectifiers and found primarily in the anterolateral portion of the BNST. Additionally, a separate population of cells was termed late-firing (LF), due to a prolonged latency to the first action potential in response to a depolarizing current trace, and was only found in the region of the oval nucleus. From our experience recording in the $BNST_{ALG}$, these late firing neurons also exhibit a strong fast inwardly rectifying current in response to hyperpolarizing current injections, suggesting they are part of the Type III classification. Additionally, there does not seem to be a separate population of Type III neurons from our sample that have a particularly long duration to the first spike (data not shown). For this reason, we believe that the LF neurons defined by Pare and colleagues can be reasonably termed Type III cells.

Despite both being in the Murinae subfamily, there were some intriguing differences in the neuronal properties and relative frequencies of the different cell types between the $BNST_{ALG}$ of the mouse and the rat. Overall, the mouse BNST cells were harder to differentiate from one another to be classified into cell types. Although there were some Type II cells in the mouse defined by the low-threshold calcium wave at the beginning of a depolarizing current injection, the calcium waves were not as pronounced as what is often seen in the rat. This makes Type II cells harder to differentiate from Type I cells. Similarly, the smaller I_h in mouse Type I cells made Type I cells hard to differentiate from Type III cells. It is possible that cells in the mouse BNST are not actually distinct populations based on their electrophysiological phenotypes, but rather exist on a continuum. The classification system for the rat $BNST_{ALG}$ was originally based on the electrophysiological phenotype alone (Hammack et al., 2007); however, it has gained credence since it was shown that $BNST_{ALG}$ neurons segregate into three distinct groups based on their mRNA expression profile for ion channel subunits using an unbiased cluster analysis and discrimination

function (Hazra et al., 2011). Moreover, we have also shown that in rats Type I–III neurons could be differentiated by their expression patterns of serotonin receptor subtype mRNA and their subsequent response to stress. However, similar comparisons were not possible in this study because the limited sequence homology for many mRNA probes from rodents to nonhuman primates precludes a direct comparison. Nevertheless, by using single cell reverse transcriptase - polymerase chain reaction (RT-PCR), and eventually single cell microarray analysis, we could better determine if distinct cell types in the mouse and non-human primate can be identified based on electrophysiological characteristics.

Similarly, although only a small percentage of Type I cells was seen in the primate and mouse relative to what is seen in the rat, it is possible that the other regular firing neurons that lack significant I_h and $I_{K(IR)}$ actually segregate into Type I cells when looking at mRNA expression profile and electrophysiological characteristics together. Appreciating how the genetic expression profile of $BNST_{ALG}$ neurons relates to the electrophysiological phenotype will be a crucial step in understanding the heterogeneity of the nucleus. We have begun to make important strides in this area in the rat. For example, serotonin receptor subtypes have been shown to be differentially expressed depending on cell type in the rat (Hazra, Guo, Dabrowska, & Rainnie, 2012). Additionally, only 15–47% of Type I and 35–53% of Type II cells express CRF mRNA whereas 81–95% of Type III neurons express the mRNA for CRF (Dabrowska, Hazra, Guo, Dewitt, & Rainnie, 2013; Dabrowska et al., 2011) and are differentially affected by chronic stress (Dabrowska, Hazra, Guo, Li, et al., 2013). These data suggest that Type III cells in the rat $BNST_{ALG}$ play a different role in the circuit than Type I and Type II cells. However, it seems unlikely that cells from the mouse and primate $BNST_{ALG}$ that fit into the classification of Type III cells are also primarily CRF neurons. In characterizing the CRF-*tomato* transgenic mouse, CRF neurons in the BNST were described as fitting into the description of Type I, Type II, and Type III cells with majority of CRF neurons not fitting into any of these categories (Silberman et al., 2013). Also, Type III cells were much more common in the primate than in the rat, how-ever, there is no evidence that the primate BNST contains more CRF neurons than the rat. This suggests that Type III neurons may not play the same role in the circuit in mouse, rat, and primates. Using single cell RT-PCR or microarray in the mouse and primate BNST would help us to understand how these cell types compare across species.

Importantly, cells with similar mRNA expression profiles across species will not necessarily display the same electrophysiological profile. Even with similar distributions of ion channels, differences in the morphology of the neurons can have significant effects on electrophysiological properties. For example, neurons with a larger dendritic surface area tend to have a smaller input resistance (Barrett & Crill, 1974). Here, we saw that there was a significant increase in total dendritic length of $BNST_{ALG}$ neurons from mouse, to rat, to primate. Interestingly, despite the drastic difference in dendritic length between mouse and primate, only rat $BNST_{ALG}$ neurons had significantly higher input resistance than the primate. When only looking at the input resistance of Type III cells, we saw that the primate Type III neurons had a significantly lower input resistance than the mouse and rat. With a more complex and extensive dendritic arbor, primate BNST neurons have a wider receptive field than BNST neurons from the mouse and rat, but a lower input resistance would suggest it would take more input to affect the cell.

In addition to affecting the input resistance, the change in dendritic arbor across species could have a drastic effect on the firing pattern of the cells. A change in dendritic surface area compared to soma/axon surface area, can significantly change the action potential waveform and firing properties of neurons, even without a change in types and densities of ion channels (Mainen & Sejnowski, 1996). With all else remaining equal, an increase in the ratio of dendritic membrane area to axo-somatic area results in a slowing of the firing rate and eventually leads to a burst-firing pattern. This could potentially contribute to the different firing patterns seen in Type II cells between mouse, rat, and primate. In the mouse, even with a prominent low-threshold calcium spike at the beginning of the depolarizing current injection, the cells tended to have a regular firing pattern. In contrast, the rat and primate Type II cells displayed more burst firing, with primate Type II cells showing the most burst firing. This could be due to a change in voltage-gated calcium channels. However, the difference in dendritic arbor suggests that the differences seen in the electrophysiological phenotypes across species could at least in part be attributed to the increase in the dendritic arbor, without significant changes in ion channel distribution.

The increase in dendritic arborization between mouse, rat, and rhesus macaque $BNST_{ALG}$ neurons suggests an increase in receptive field for these cells. Importantly, there is evidence that the connectivity of the BNST with the rest of the brain has been largely conserved from rodents to nonhuman and human primates alike with the major fiber tracks consisting of (a) the posterior bundle (stria terminalis), connecting the BNST to the thalamus and lateral amygdala, (b) the ventral bundle (ansa peduncularis), connecting the BNST to the basal forebrain and medial amygdala (Avery et al., 2014; Dong, Petrovich, Petrovich, Swanson, & Swanson, 2001; Dong, Petrovich, Petrovich, Watts, et al., 2001; Dong & Swanson, 2004; Krüger, Shiozawa, Kreifelts, Scheffler, & Ethofer, 2015), and (c) the anterior bundle which connects the BNST to the nucleus accumbens and prefrontal cortex, but in primates, extends to include the orbitofrontal cortex (OFC), a region important in decision making (Krüger et al., 2015). The ventromedial prefrontal cortex (vmPFC), which includes the OFC, has recently been shown to modulate the BNST in humans, providing further support for a structural and functional connection between the OFC and BNST in humans (Motzkin et al., 2015). Lesions of the OFC in monkeys altered anxiety behavior and BNST metabolism, suggesting that this connection between the BNST and OFC exists in nonhuman primates as well (Fox et al., 2010). Additionally, the stria terminalis, or posterior bundle, extends beyond the amygdala and into the temporal pole in humans (Avery et al., 2014; Krüger et al., 2015). These new connections of the primate BNST to other areas of the brain not observed in rodents suggests an evolutionary pressure for the primate BNST to adapt to an increase in diversity of inputs and projections as the cortex expands and diversifies. It is possible this pressure resulted in an increase in the complexity of the dendritic arbor and the heterogeneity of cell types. Interestingly, the electrophysiological phenotype in the $BNST_{ALG}$ in the primate is potentially less diverse than that seen in the rat, as the majority of cells look like Type III neurons. However, there are also potential new cell types from those seen in the rat, such as the stutter firers and neurons with large fAHPs. Most likely, single cell microarray analysis in the primate would reveal an increase in heterogeneity in cell type compared to the rat. Future studies using more targeted manipulations, such as

optogenetic activation of afferents from defined upstream sites, may reveal subtle nuances of cell type-selective input across species.

In conclusion, we have described the electrophysiological phenotype of neurons in the $BNST_{ALG}$ of the mouse and rhesus macaque using the classification system set forth for neurons in the rat $BNST_{ALG}$. Both the mouse and primate $BNST_{ALG}$ contained cells that closely fit the description of Type I, Type II, and Type III cells in the rat; however, they were observed in significantly different proportions. Additionally, we showed that the dendritic arbor becomes significantly more complex from the mouse to the rat to the primate. These data suggest that electrophysiological cell types should be used with caution when looking at different species.

There are some limitations in this study. For example, although we have gathered data from numerous cells, the sample size of particular cell types, namely Type I cells in the primate and the “other” cells in the primate and mouse, are too small to be able to draw firm conclusions about their physiological properties and relative frequency in the nucleus. Additionally, it is unclear whether the differences in the electrophysiological phenotypes across species directly result in a functional difference. However, in the rat, these electrophysiological phenotypes seem to reflect functional differences in the role the cells play in the circuit, as demonstrated by differences in gene expression and the response to stress. The results reported here suggest that the observations related to specific cell types reported in the rat should not be assumed to also occur in the mouse or primate. Indeed, we were surprised to see that the cell types in the mouse and primate seemed more similar to one another than the cell types of the mouse and rat or rat and primate. However, several factors could play into this apparent mismatch. For example, we know that monoamine neuro-transmitters play a key neurotrophic role during neuronal development. However, immunohistochemical studies of 5-HTT expression show that in the rat and nonhuman-primate, the distribution of serotonergic fibers shows high regional selectivity, which is not the case in the majority of mouse strains (Bauman & Amaral, 2005; Linley, Olucha-Bordonau, & Vertes, 2017; O’Rourke & Fudge, 2006; Shigematsu, Yamamoto, Higuchi, & Fukuda, 2006). Hence, one might have expected a greater similarity in the physiology of BNST neurons between rat and nonhuman primate. An additional, consideration is that the data obtained from rat and mouse were collected from animals 40–60 days old, which is equivalent to late adolescence/early adulthood in rodents. In contrast, because of restriction to access, the primate tissue was obtained from animals 14–40 months, with a modal age of ~18 months, which corresponds to early adolescence. It is possible that age-matched rat and nonhuman primate BNST neurons may show a similar physiologic profile, but this is beyond the scope of the current investigation.

Importantly, there are multiple factors that go into the electro-physiological phenotype of a neuron, including morphology and ion channel expression and distribution. Although the electrophysiological phenotypes of the cells differ across species, there may still be analogous cell types in the different species, potentially better classified based on their mRNA expression profile. Future studies should examine cell types in the $BNST_{ALG}$ of the mouse, rat, and primate using a combination of electrophysiology and single cell RT-PCR or microarray to better understand differences in the circuitry across species.

Acknowledgments

Funding information

National Institutes of Health, Grant number: MH-072908 and 5F31MH-097331; National Institutes of Health's Office of the Director, Office of Research Infrastructure Programs, Grant number: P51OD011132

References

Alvarez RP, Chen G, Bodurka J, Kaplan R, Grillon C. Phasic and sustained fear in humans elicits distinct patterns of brain activity. NeuroImage. 2011; 55:389–400. [PubMed: 21111828]

Avery SN, Clauss JA, Winder DG, Woodward N, Heckers S, Blackford JU. BNST neurocircuitry in humans. NeuroImage. 2014; 91:311–323. [PubMed: 24444996]

Barrett JN, Crill WE. Specific membrane properties of cat motoneurones. The Journal of Physiology. 1974; 239:301–324. [PubMed: 4137933]

Bauman MD, Amaral DG. The distribution of serotonergic fibers in the macaque monkey amygdala: An immunohistochemical study using antisera to 5-hydroxytryptamine. Neuroscience. 2005; 136:193–203. [PubMed: 16182456]

Bota M, Sporns O, Swanson LW. Neuroinformatics analysis of molecular expression patterns and neuron populations in gray matter regions: The rat BST as a rich exemplar. Brain Research. 2012; 1450:174–193. [PubMed: 22421015]

Dabrowska J, Hazra R, Ahern TH, Guo JD, McDonald AJ, Mascagni F, … Rainnie DG. Neuroanatomical evidence for reciprocal regulation of the corticotrophin-releasing factor and oxytocin systems in the hypothalamus and the bed nucleus of the stria terminalis of the rat: Implications for balancing stress and affect. Psychoneuroendocrinology. 2011; 36:1312–1326. [PubMed: 21481539]

Dabrowska J, Hazra R, Guo JD, Dewitt S, Rainnie DG. Central CRF neurons are not created equal: Phenotypic differences in CRF-containing neurons of the rat paraventricular hypothalamus and the bed nucleus of the stria terminalis. Frontiers in Neuroscience. 2013; 7:156. [PubMed: 24009552]

Dabrowska J, Hazra R, Guo JD, Li CC, Dewitt S, Xu J, … Rainnie DG. Striatal-enriched protein tyrosine phosphatase-STEPs toward understanding chronic stress-induced activation of corticotrophin releasing factor neurons in the rat bed nucleus of the stria terminalis. Biological Psychiatry. 2013; 74:817–826. [PubMed: 24012328]

Dong, HW. Allen reference atlas: A digital color brain atlas of the C57BL/6J male mouse. Hoboken, New Jersey: John Wiley & Sons; 2007.

Dong HW, Petrovich GD, Petrovich GD, Swanson LW, Swanson LW. Topography of projections from amygdala to bed nuclei of the stria terminalis. Brain Research Reviews. 2001; 38:192–246. [PubMed: 11750933]

Dong HW, Petrovich GD, Petrovich GD, Watts AG, Watts AG, Swanson LW, Swanson LW. Basic organization of projections from the oval and fusiform nuclei of the bed nuclei of the stria terminalis in adult rat brain. Journal of Comparative Neurology. 2001; 436:430–455. [PubMed: 11447588]

Dong HW, Swanson LW. Organization of axonal projections from the anterolateral area of the bed nuclei of the stria terminalis. Journal of Comparative Neurology. 2004; 468:277–298. [PubMed: 14648685]

Duvarci S, Bauer EP, Pare D. The bed nucleus of the stria terminalis mediates inter-individual variations in anxiety and fear. Journal of Neuroscience. 2009; 29:10357–10361. [PubMed: 19692610]

Ehrlich DE, Ryan SJ, Rainnie DG. Postnatal development of electrophysiological properties of principal neurons in the rat basolateral amygdala. The Journal of Physiology. 2012; 590:4819–4838. [PubMed: 22848043]

Fox AS, Shelton SE, Oakes TR, Converse AK, Davidson RJ, Kalin NH. Orbitofrontal cortex lesions alter anxiety-related activity in the primate bed nucleus of stria terminalis. Journal of Neuroscience. 2010; 30:7023–7027. [PubMed: 20484644]

Francesconi W, Berton F, Repunte-Canonigo V, Hagihara K, Thurbon D, Lekic D, … Sanna PP. Protracted withdrawal from alcohol and drugs of abuse impairs long-term potentiation of intrinsic excitability in the juxtacapsular bed nucleus of the stria terminalis. Journal of Neuroscience. 2009; 29:5389–5401. [PubMed: 19403807]

Guo JD, Hammack SE, Hazra R, Levita L, Rainnie DG. Bi-directional modulation of bed nucleus of stria terminalis neurons by 5-HT: Molecular expression and functional properties of excitatory 5-HT receptor subtypes. Neuroscience. 2009; 164:1776–1793. [PubMed: 19778589]

Hammack SE, Mania I, Rainnie DG. Differential expression of intrinsic membrane currents in defined cell types of the anterolateral bed nucleus of the stria terminalis. Journal of Neurophysiology. 2007; 98:638–656. [PubMed: 17537902]

Hazra R, Guo JD, Dabrowska J, Rainnie DG. Differential distribution of serotonin receptor subtypes in BNST(ALG) neurons: Modulation by unpredictable shock stress. Neuroscience. 2012; 225:9–21. [PubMed: 22922122]

Hazra R, Guo JD, Ryan SJ, Jasnow AM, Dabrowska J, Rainnie DG. A transcriptomic analysis of type I–III neurons in the bed nucleus of the stria terminalis. Molecular and Cellular Neuroscience. 2011; 46:699–709. [PubMed: 21310239]

Ju G, Swanson LW, Simerly RB. Studies on the cellular architecture of the bed nuclei of the stria terminalis in the rat: II. Chemoarchitecture. Journal of Comparative Neurology. 1989; 280:603–621. [PubMed: 2468695]

Kalin NH, Shelton SE, Fox AS, Oakes TR, Davidson RJ. Brain regions associated with the expression and contextual regulation of anxiety in primates. Biological Psychiatry. 2005; 58:796–804. [PubMed: 16043132]

Krüger O, Shiozawa T, Kreifelts B, Scheffler K, Ethofer T. Three distinct fiber pathways of the bed nucleus of the stria terminalis to the amygdala and prefrontal cortex. Cortex. 2015; 66:60–68. [PubMed: 25800506]

Larriva-Sahd J. Histological and cytological study of the bed nuclei of the stria terminalis in adult rat. II. Oval nucleus: Extrinsic inputs, cell types, neuropil, and neuronal modules. Journal of Comparative Neurology. 2006; 497:772–807. [PubMed: 16786552]

Linley SB, Olucha-Bordonau F, Vertes RP. Pattern of distribution of serotonergic fibers to the amygdala and extended amygdala in the rat. Journal of Comparative Neurology. 2017; 525:116–139. [PubMed: 27213991]

Macey DJ, Smith HR, Nader MA, Porrino LJ. Chronic cocaine self-administration upregulates the norepinephrine transporter and alters functional activity in the bed nucleus of the stria terminalis of the rhesus monkey. Journal of Neuroscience. 2003; 23:12–16. [PubMed: 12514195]

Mainen ZF, Sejnowski TJ. Influence of dendritic structure on firing pattern in model neocortical neurons. Nature. 1996; 382:363–366. [PubMed: 8684467]

Mantsch JR, Vranjkovic O, Twining RC, Gasser PJ, McReynolds JR, Blacktop JM. Neurobiological mechanisms that contribute to stress-related cocaine use. Neuropharmacology. 2014; 76(Pt B): 383–394. [PubMed: 23916481]

Molineux ML, Fernandez FR, Mehaffey WH, Turner RW. A-type and T-type currents interact to produce a novel spike latency-voltage relationship in cerebellar stellate cells. Journal of Neuroscience. 2005; 25:10863–10873. [PubMed: 16306399]

Motzkin JC, Philippi CL, Oler JA, Kalin NH, Baskaya MK, Koenigs M. Ventromedial prefrontal cortex damage alters resting blood flow to the bed nucleus of stria terminalis. Cortex. 2015; 64:281–288. [PubMed: 25569763]

Muly EC, Senyuz M, Khan ZU, Guo JD, Hazra R, Rainnie DG. Distribution of D1 and D5 dopamine receptors in the primate and rat basolateral amygdala. Brain Structure and Function. 2009; 213:375–393. [PubMed: 19669160]

O'Rourke H, Fudge JL. Distribution of serotonin transporter labeled fibers in amygdaloid subregions: Implications for mood disorders. Biological Psychiatry. 2006; 60:479–490. [PubMed: 16414028]

Paxinos, G., Huang, XF., Toga, AW. The rhesus monkey brain in stereotaxic coordinates. San Diego, CA: Academic Press; 2000.

Paxinos, G., Watson, C. The rat brain in stereotaxic coordinates (Compact). 3. San Diego, CA: Academic Press; 1996.

Pleil KE, Lowery-Gionta EG, Crowley NA, Li C, Marcinkiewcz CA, Rose JH, … Kash TL. Effects of chronic ethanol exposure on neuronal function in the prefrontal cortex and extended amygdala. Neuropharmacology. 2015; 99:735–749. [PubMed: 26188147]

Pleil KE, Rinker JA, Rinker JA, Lowery-Gionta EG, Lowery-Gionta EG, Mazzone CM, … Kash TL. NPY signaling inhibits extended amygdala CRF neurons to suppress binge alcohol drinking. Nature Neuroscience. 2015; 18:545–552. [PubMed: 25751534]

Rodriguez-Sierra OE, Rodríguez-Sierra OE, Turesson HK, Pare D. Contrasting distribution of physiological cell types in different regions of the bed nucleus of the stria terminalis. Journal of Neurophysiology. 2013; 110:2037–2049. [PubMed: 23926040]

Ryan SJ, Ehrlich DE, Jasnow AM, Daftary S, Madsen TE, Rainnie DG. Spike-timing precision and neuronal synchrony are enhanced by an interaction between synaptic inhibition and membrane oscillations in the amygdala. PLoS One. 2012; 7:e35320. [PubMed: 22563382]

Ryan SJ, Ehrlich DE, Rainnie DG. Morphology and dendritic maturation of developing principal neurons in the rat basolateral amygdala. Brain Structure and Function. 2014; 221:839–854. [PubMed: 25381464]

Shigematsu N, Yamamoto K, Higuchi S, Fukuda T. Novel non-uniform distribution of serotonin transporter in the mouse hippocampus and neocortex revealed by N- and C- terminal domain-specific immunohistochemistry. Brain Research. 2006; 1075:110–116. [PubMed: 16460713]

Silberman Y, Matthews RT, Winder DG. A corticotropin releasing factor pathway for ethanol regulation of the ventral tegmental area in the bed nucleus of the stria terminalis. Journal of Neuroscience. 2013; 33:950–960. [PubMed: 23325234]

Somerville LH, Whalen PJ, Kelley WM. Human bed nucleus of the stria terminalis indexes hypervigilant threat monitoring. Biological Psychiatry. 2010; 68:416–424. [PubMed: 20497902]

Straube T, Mentzel HJ, Miltner WHR. Waiting for spiders: Brain activation during anticipatory anxiety in spider phobics. NeuroImage. 2007; 37:1427–1436. [PubMed: 17681799]

Sullivan GM, Apergis J, Bush DEA, Johnson LR, Hou M, Ledoux JE. Lesions in the bed nucleus of the stria terminalis disrupt corticosterone and freezing responses elicited by a contextual but not by a specific cue-conditioned fear stimulus. Neuroscience. 2004; 128:7–14. [PubMed: 15450349]

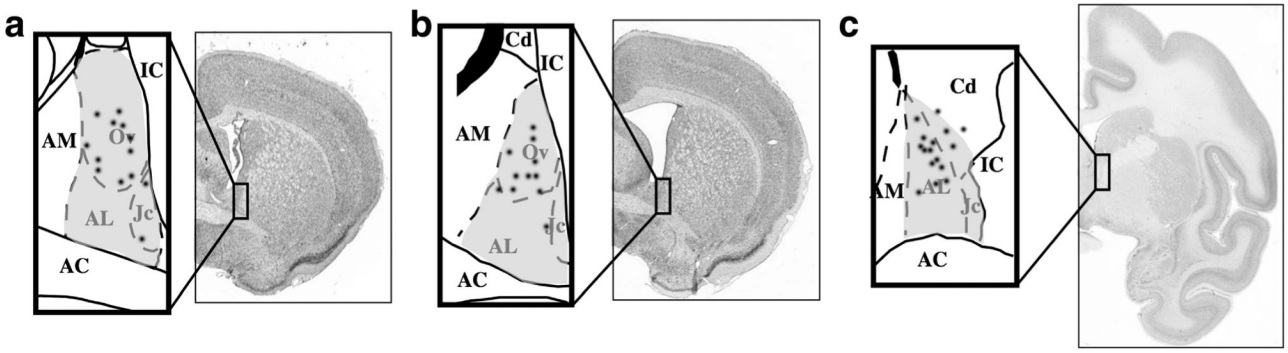

FIGURE 1.

The anterior BNST in the mouse (a), rat (b), and rhesus macaque (c). Adapted from Dong (2007), Paxinos and Watson (1996), and Paxinos, Huang, and Toga (2000), respectively. Shaded regions represent recording area. Black dots represent the approximate recording locations verified from the biocytin-filled cells. Dark region is the lateral ventricle. Abbreviations: AC =anterior commissure; AL =anterolateral BNST; AM =anteromedial BNST; Cd =caudate; IC =internal capsule; Jc =juxtacapsular BNST; Ov =oval BNST

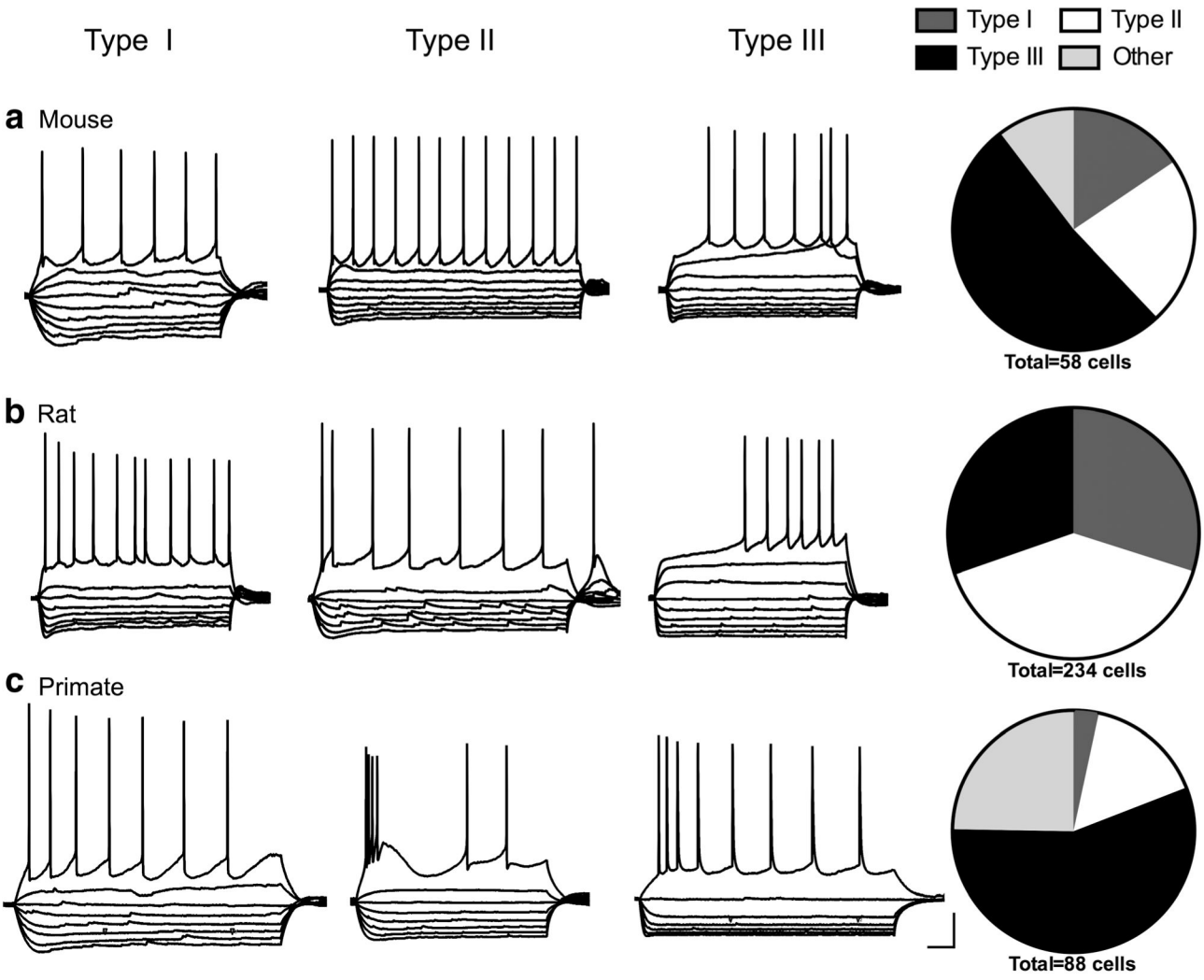

FIGURE 2.

Example voltage response to hyperpolarizing and depolarizing current injections and relative frequency of Type I, II, and III cells in the mouse (a), rat (b), and primate (c) BNST displayed in pie charts. Scale bar: 20 mV and 100 ms

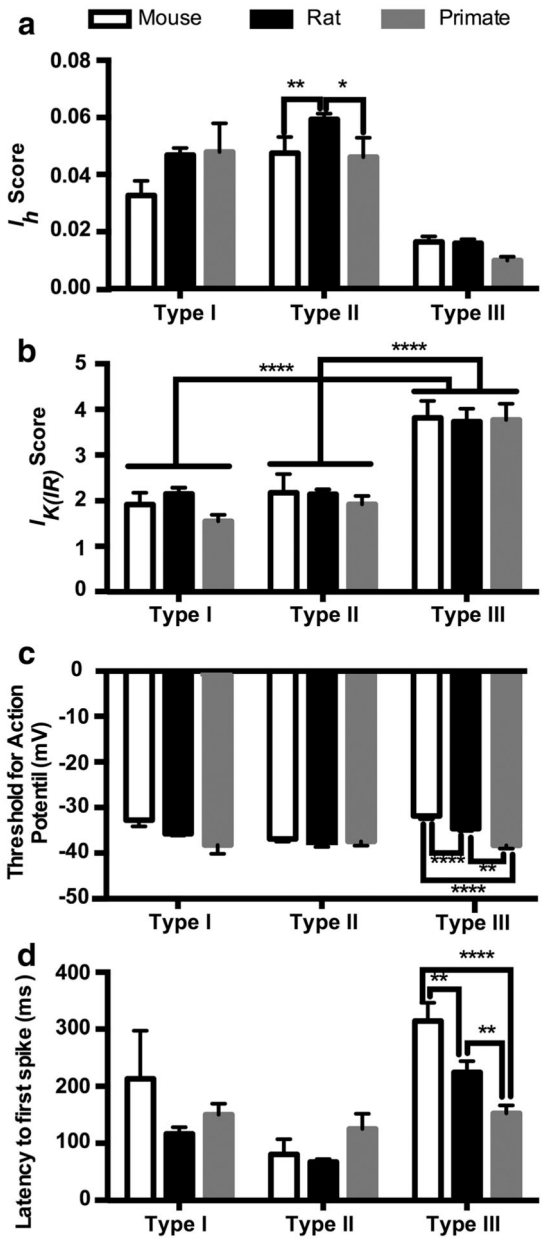

FIGURE 3.

Comparison of electrophysiological properties of Type I, II, and III neurons in the mouse, rat, and primate BNST. Plots of the and I_h score (a), $I_{K(IR)}$ score (b), threshold for action potential generation (c), and latency to first spike (d). *p <.05, **p <.01, ****p <.0001. Comparisons between cell types not shown for I_h and latency to first spike

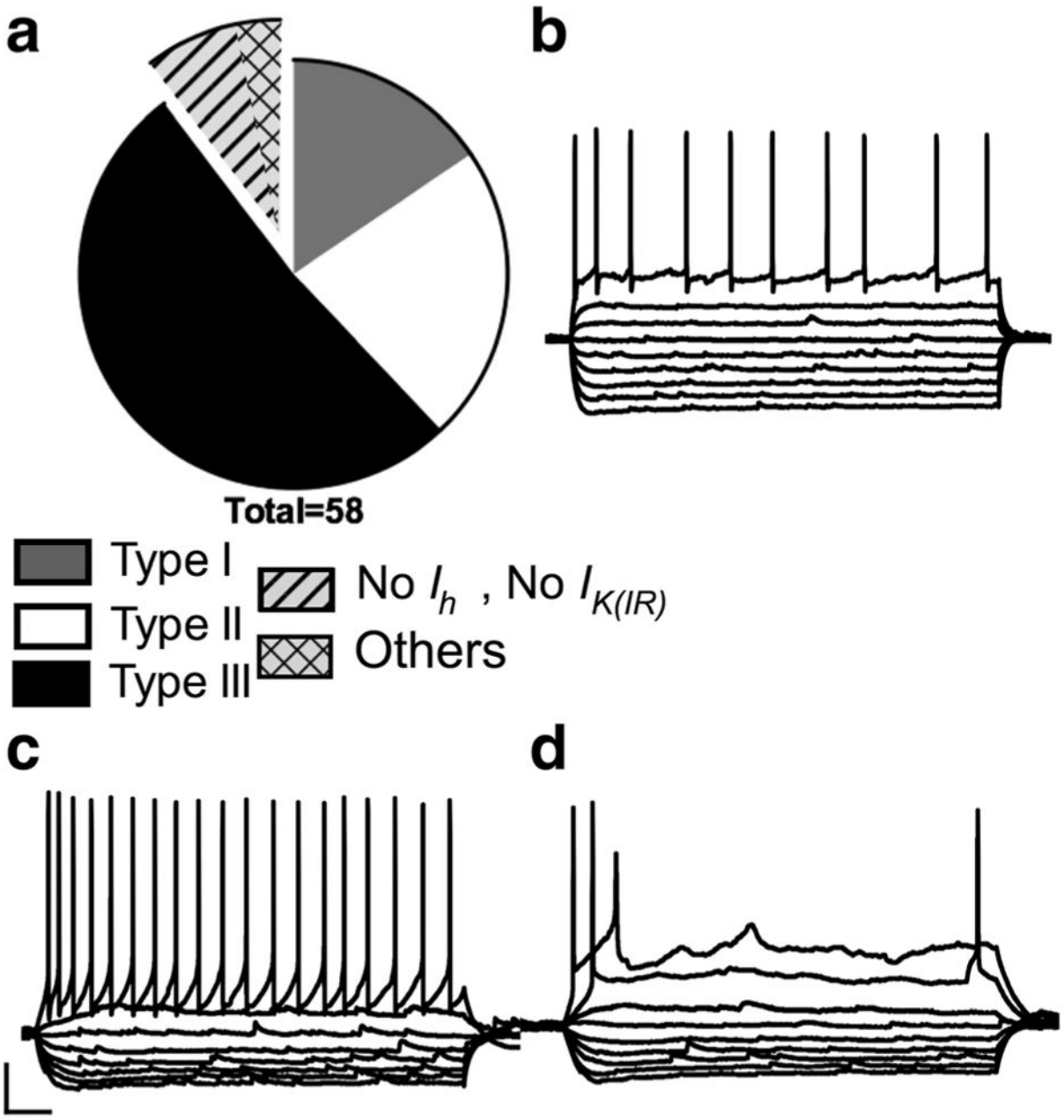

FIGURE 4.

Relative frequency and example voltage traces of mouse neurons that do not fit into the classification of Type I, II, or III. Exploded portion of the pie chart shows the relative contribution of regular spiking (RS) cells without much I_h or $I_{K(IR)}$ to the "others" category (a) and (b) shows a voltage trace from an example neuron from this group. Panels (c) and (d) show voltage traces from two neurons that did not fit into any classification system. Scale bar: 20 mv and 100 ms

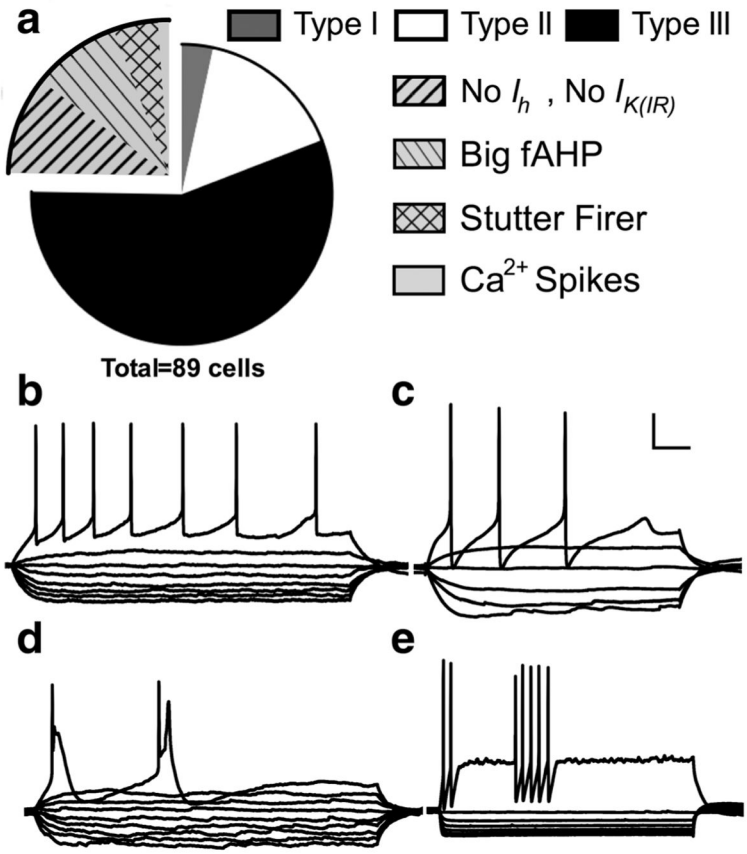

FIGURE 5.

Relative frequency and example voltage traces of primate neurons that do not fit into the classification of Type I, II, or III. Exploded portion of the pie chart shows the relative contribution of the different cell groups to describe the neurons classified as “other” (a). Example voltage traces of a neuron from each group: a RS cell without much I_h or $I_{K(IR)}$ (b), neurons with a large fAHP (c), neurons with large low-threshold calcium spikes (d), and neurons with a stutter firing pattern (e). Scale bar: 20 mv and 100 ms

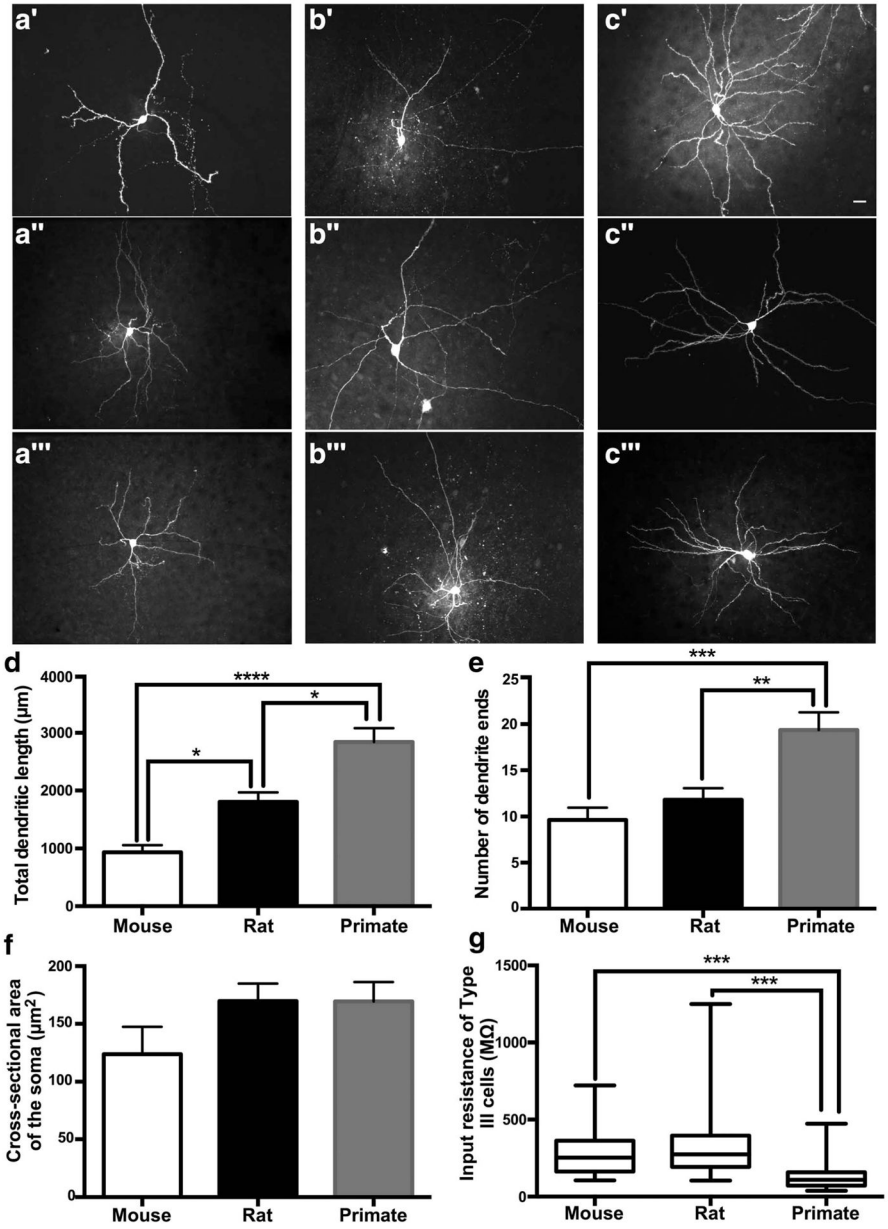

FIGURE 6.

Neuronal morphology and input resistance of mouse, rat, and primate cells in the BNST. Example maximum projections of z-stack images cells from the mouse (a′–a‴), rat (b′–b‴), and primate (c′–c‴) BNST (white scale bar is 20 µm). Plot of the total dendritic length (d), number of dendrite ends (e), area of the cell body (f), and input resistance of Type III cells (g). Scale bars are *SEM*. **p* <.05, ***p* <.01, ****p* <.001, *****p* <.0001

TABLE 1

Basic electrophysiological properties of Type I, Type II, and Type III cells in the mouse, rat, and primate.

	Mouse			Rat			Primate		
	I	**II**	**III**	**I**	**II**	**III**	**I**	**II**	**III**
Number of animals	5	8	13	37	35	44	3	3	8
Sample size (cells)	7	13	30	69	94	70	3	14	49
Threshold (mV)	−32.8 ±1.4	−36.9 ±0.6	−31.9 ±0.7	−35.8 ±0.4	−38.2 ±0.4	−34.6 ±0.5	−39.0 ±2.0	−37.4 ±1.0	−38.5 ±0.7
Spike latency (ms)	213.2 ±92.3	80.6 ±26.5	314.1 ±32.3	116.6 ±11.6	67.3 ±5.0	224.5 ±19.7	150.2 ±19.5	124.8 ±26.6	154.3 ±14.1
I_h score	0.033 ±0.006	0.047 ±0.006	0.016 ±0.002	0.047 ±0.002	0.059 ±0.002	0.016 ±0.001	0.048 ±0.010	0.046 ±0.007	0.010 ±0.001
$I_{K(IR)}$ score	1.92 ±0.69	2.18 ±0.40	3.82 ±0.37	2.15 ±0.13	2.14 ±0.11	3.73 ±0.29	1.55 ±0.15	1.92 ±0.19	3.79 ±0.36
R_{in} (MΩ)	376.7 ±72.7	328.2 ±34.0	277.1 ±27.0	388.1 ±25.6	331.9 ±15.0	359.5 ±36.3	798.5 ±516.8[a]	332.1 ±57.1	141.1 ±15.0

Note. Average ±*SEM*.

[a]Sample size for Type I primate cells is small, and average and SEM may not represent the data fairly.

TABLE 2

Relative frequency of cell types seen in the anterolateral BNST of the rat from the recent sample and previously published papers (Hammack et al., 2007; Hazra et al., 2011; Rodriguez-Sierra et al., 2013).

	Type I (RS)	Type II (LTB)	Type III (fIR)	LF (also type III)
Current sample	29.5%	40.2%	30.3%	
Hammack et al. (2007)	29%	55%	16%	
Hazra et al. (2011)	11%	66%	21%	
Rodriguez-Sierra et al. (2013)[b]	24.9%	54.5%	16.5%	1.7%[a]

The following are acronyms given by Rodriguez-Sierra et al (2013): RS =regular spiking; LTB =low-threshold bursting; fIR =fast inward rectification; LF =late firing.

[a]These cells are most likely a part of the classification of Type III in our classification scheme.

[b]From the anterior BNST, including the medial BNST and ventral BNST.